NASA Contractor Report

A Semi-Micromechanic Interlaminar Strain Analysis on Curved-Beam Specimens

Duksung Joh

Deparment of Mechanical and Aerospace Engineering and
Engineering Mechanics
University of Missouri-Rolla, Rolla, Missouri 65401-0249

Final Report,
April-December 31 1990
under Grant NCC 2-673

ABSTRACT

Experimental Analyses were performed for determination of interlaminar strains in circumferentially unidirectional curved-beam specimens. Semi-circular and semi-elliptic carbon/epoxy specimens were subjected to opening-mode tensile loadings. Whole-field measurements were recorded at load levels from about 5 % to more than 90 % of failure loads.

Contour maps of displacement fields were obtained by using moire interferometry, using reference gratings of 2,400 lines/mm or 60,690 lines/in. Whole-field contour maps of circumferential and interlaminar strains were obtained by using moire interferometry in a semi-micromechanic scale.

Various anomalous effects were observed in the displacement fields. The zig-zag fringe patterns indicated that the fiber orientation in each layer was not truly circumferential. This deviation from the unidirectionality caused free-edge effects, such as interlaminar shear strains even at the axis of symmetry and the altered normal strains in the thickness direction. In the resin-rich zones between layers, the tensile interlaminar strain was excessively large due to the large compliance. As the result of the combined effect of these anomalous behaviors, the values of the interlaminar tensile strains were larger than those predicted analytically. The modulus E_3 was actually smaller than the assumed value E_2 by 20 %.

INTRODUCTION

Delamination in laminated composite plates has been recognized as one of the most critical failure mechanisms in advanced composite structures, as composite laminates are not reinforced in the through-the-thickness direction. The ultimate goal of delamination study is to design a composite laminate which has a high value of interlaminar strength. Prior to any attempt of developing a new concept to enhance interlaminar strength, however, the mechanical interlaminar behavior of composite laminates must be characterized experimentally as well as analytically. In particular, interlaminar tensile stresses developed inherently in curved laminates need to be studied thoroughly because these stresses can greatly limit the versatility of composites in structural applications when the laminates are not reinforced properly for the interlaminar stresses. Unfortunately, however, the interlaminar stress/strain analysis for curved plates has been one of the least-studied research topics for composite laminates.

With a growing employment of curved-plate geometry in composite structures, the study on interlaminar strength and delaminations has received more attention. Due to the limited capabilities of conventional methods of experiments, post-delamination observations have mainly been the approaches for the analysis of these phenomena, whereas the study of deformations prior to delaminations is essential to understanding of the mechanical response of the materials, and eventually, to development of new materials. Quantitative nondestructive testing methods to measure the highly localized strains and stresses have not been available.

The objective of this research was quantitative measurements of strains varying through the thickness of the semi-circular and semi-elliptic carbon/epoxy specimens. A relatively new concept of quantitative nondestructive evaluation, high-sensitivity

moire interferometry, was developed further to measure the highly localized strains varying through the thickness of curved plates at the region of maximum curvature. Whole-field contour maps of deformations and strains were obtained in semi-micromechanic scale.

Various anomalous effects were observed and interpreted. Experimental measurements, the first achievement in this area, will provide designers of composite structures with the practical empirical data needed to understand the mechanism of the initiation of delaminations in curved sections of composite laminates.

SPECIMENS AND LOADING

Two specimen configurations were used in this study; semi-circular and semi-elliptic, as shown in Figure 1. The semi-elliptic specimens were made with T300/934 Graphite/Epoxy, and the semi-circular specimens were made with G40-600/5245C Graphite/Modified Epoxy. Both are curved beams with all plies oriented in the circumferential direction (100% 0° layup). The unidirectional stacking sequence eliminates the free-edge interlaminar tensile stresses that would occur for other stacking sequences as load is applied or during cooldown from the cure temperature. The specimens were provided by NASA Ames Research Center. Their edge surfaces were ground flat at the University of Missouri-Rolla by surface grinding. A special care was taken to ensure that the sharp edges were not rounded.

Some semi-elliptic specimens showed manufacturing defects caused by the fibers squeezed out through the gap between the split molds. In Fig. 2, the enlarged picture of the cross-section of the defect is shown very clearly. Reasonably good specimens were selected by using a microscope. Semi-circular specimens were free of defects because the split molds were not used for these specimens.

To apply the load to the curved specimens, rigid tabs were clamped at the two ends of the specimens, as shown in Fig. 3. The tensile load was applied to the specimens quasi-statically by using two pins attached to the loading grips. This loading configuration was employed in order to avoid the moment developed by the conventional loading grips. Since the deformation or the pin deflection was very large in the semi-elliptic specimens, the tabs were fixed by bolts and nuts through the holes in the specimens to prevent slipping of the tabs at high load levels.

The loading had to be stopped periodically to take the pictures of the moire fringe patterns of deformations in the specimens. A table-top load frame was fabricated at the University of Missouri-Rolla to be used on the optical table of moire interferometry.

MOIRE INTERFEROMETRY

Moire interferometry is a whole-field optical method using coherent laser light to measure in-plane displacements. A comprehensive description appears in a few references.[1,2] Briefly, a high frequency crossed-line diffraction grating is replicated on the specimen surface using a special mold. The result is a thin reflective phase grating firmly adhered to the specimen, which deforms together with the specimen surface. The specimen grating is observed in an optical arrangement illustrated in Fig. 4. Two beams of light incident at angles α and $-\alpha$ form a virtual reference grating. Its frequency is $f = (2 \sin \alpha)/\lambda$, where λ is the wavelength of the light. This reference grating interacts with the specimen grating to form the two-beam interference pattern viewed in the camera. The pattern is a contour map of displacements governed by the relationship

$$U = \frac{1}{f} N_x \tag{1}$$

where U is the in-plane x-component of displacement at any point, and N_x is the fringe order at that point in the fringe pattern, obtained when the reference grating lines are perpendicular to the x-axis.

In this work, the grating was applied in the xy plane with lines perpendicular to the x- and y-axes. The alignment of the grating lines was done by using the flat part of the specimens as a guide. In-plane displacements, V, in the y-directionare obtained from fringe orders, N_y, obtained from the orthogonal grating by

$$V = \frac{1}{f} N_y \tag{2}$$

Frequency f was 60,960 lines /in. (2,400 lines/mm), which gave a sensitivity of U and V measurements of 16.4 μin. (0.417 μm) per fringe order. A He/Ne laser was used at wavelength 0.633 μm and 10 mW power.

Another laser was used in the optical arrangement of Fig. 4. Due to the non-rigid grips and the relatively flexible pin fixtures, the specimen-face orientation was not stable as the load was increased. When the direction of the specimen grating changes, the density of the fringes in the displacement patterns changes. In other words, the original optical alignment is altered with the load increase. In order to insure the specimen grating to face in the fixed direction, there should be a means to monitor the face angle of the specimen. A laser beam from the second laser is reflected from the specimen grating, and the zero-diffraction order beam is marked on the wall in the laboratory after all the optical elements are aligned properly. As the load was increased, it could be observed that the beam drifted on the wall. The face of the

specimen was readjusted to its original angle by using the alignment beam and the mark on the wall. The loading frame was rotated about the two axes by using the three screws on it in the process of readjustment.

EXPERIMENTAL PROCEDURE

A preliminary series of tests was performed on the two types of specimens to measure the strains. For each test, a high-frequency crossed-line grating was applied to the flat edge of the specimen. The specimen was installed in the table-top loading frame and the optical set-up was aligned for a null-fringe field before the specimen was loaded. From the preliminary test data provided by NASA Ames, the load increment was determined. The preliminary tests were conducted without the secondary laser, which was later used for the purpose of maintaining the fixed orientation of the specimen surface. The result showed that the direction of the specimen grating was changing continuously altering the effective grating frequency significantly. The apparent tensile strain in the thickness direction was excessively large. When the strain field was converted to the stress field, the tensile stress in the thickness direction was about 20 % higher than those values obtained by analytical solutions. This deviation could be caused by the two effects; mis-orientation of the specimen surface in loading and the assumption of $E_2 = E_3$.

In the subsequent series of tests, the secondary laser was used to eliminate the effect of mis-orientation of the specimen surface in loading. After each increment of load, the specimen face was re-oriented in its original direction of the null-fringe alignment, and the U and V patterns were photographed. The 4″×5″ sheet films and the 4″-aperture camera lens were used.

RESULTS

The fringe patterns are shown in Figs. 5-8. In all the V patterns, the fringes are zig-zag shaped, which is characteristic of the free-edge deformations of non-unidirectional laminates. This shows that the layers were not unidirectionally stacked when the laminates were fabricated, which is practically very difficult to achieve. Since the measurements are performed at the free edge, the free-edge deformations can cause some error to a certain degree. In this research, however, the angular deviations of the fibers or layers from the circumferential direction were assumed to be negligibly small.

In the U patterns for the semi-elliptical specimens, anomalous effects were exhibited, manifest as irregular fringes near the outer edge of the maximum-curvature region. These irregularities were caused by the manufacturing defects, the locally increased curvature of the aligned fibers near the gap between the two split molds.

Strains were determined along the axis of symmetry by using the equations

$$\varepsilon_x = \frac{\delta U}{\delta x} \approx \frac{1}{f}\left(\frac{\Delta N_x}{\Delta x}\right) MF$$
$$\varepsilon_y = \frac{\delta V}{\delta y} \approx \frac{1}{f}\left(\frac{\Delta N_y}{\Delta y}\right) MF \qquad (3)$$

where ΔN_x and Δ_y are the fringe order difference between the two fringes, respectively for the two fringe patterns, Δx and Δy are the distances between the fringes, and MF is the magnification factor of the fringe patterns.

The resulting strains are shown in Figs. 9-18. In Fig. 9, the interlaminar tensile strain, ε_x, for the semi-elliptic specimens are shown, with all the data points connected linearly, for the two load levels. The peak strain values in the figure indicate that the soft resin-rich zones between layers deformed excessively in tension. In Fig. 10, the

same strains are plotted by using the cubic-spline method. This figure also shows the same irregularities as in Fig. 9. The moire interferometry technique has such a high spatial resolution that the resulting strain distribution is semi-micromechanic. The assumption of homogeneous material properties, which is commonly adopted in analytical solutions, is not valid anymore in this experiment. It is not quite reasonable to use this strain data with the conventional constitutive relationships to determine stresses because the stiffnesses are not constant at all when considered in the same scale. The strain data was curve-fitted by using a fourth-order polynomial, as shown in Fig. 11.

The circumferential strains, ε_y, are shown for the two load levels in Fig. 12 along the axis of symmetry. The irregularities of the curves are less severe than those for the strain, ε_x. In Fig. 13, the two strains, ε_x and ε_y, are compared for the same load, 150 lb.

The semi-circular specimens showed the behaviors similar to those of the semi-elliptic specimens. In Fig. 14, the interlaminar tensile strains are plotted for the two load levels. The peak strains at the soft interlaminar layers are intensified as the load is increased. The cubic-spline fitting of the data points, as shown in Fig. 15, also shows the same behavior. When a fourth-order polynomial was used, the behavior was smoothed as shown in Fig. 16.

The circumferential strains, ε_y, are shown for the two load levels in Fig. 17 along the axis of symmetry. The irregularities of the curves are less severe than those for the strain, ε_x. In Fig. 18, the two strains, ε_x and ε_y, are compared for the same load, 155 lb.

To compare the experimental results with the anlytical solutions, the stresses were determined by using the approximately smoothed data and the two dimensional

constitutive relationships for the semi-circular specimens only. As the shear stresses can be neglected in the material principal directions on the axis of symmetry, the constitutive relationship is reduced to

$$\begin{Bmatrix} \sigma_x \\ \sigma_y \end{Bmatrix} = \begin{bmatrix} Q_{11} & Q_{12} \\ Q_{12} & Q_{22} \end{bmatrix} \begin{Bmatrix} \varepsilon_x \\ \varepsilon_y \end{Bmatrix} \tag{4}$$

where the Q_{ij} are the reduced stiffnesses in which $E_3 = E_2$ was assumed. The analytical solutions were obtained by NASTRAN and the exact solution by Lekhnitskii.[3] The large discrepancy was observed between the solutions near the outer edge, which is believed to have been caused by the structural defect of the specimen at this region. The maximum stresses were compared between the solutions. The stress by anlytical solutions was 80 % of the stress by the experiment.

DISCUSSION AND CONCLUSIONS

Experimental Analyses were performed for determination of interlaminar strains in circumferentially unidirectional curved-beam specimens. Semi-circular and semi-elliptic carbon/epoxy specimens were subjected to opening-mode tensile loadings. Whole-field measurements were recorded at various load levels.

Contour maps of displacement fields were obtained by using moire interferometry, using reference gratings of 2,400 lines/mm or 60,690 lines/in. Whole-field contour maps of circumferential and interlaminar strains were obtained by using moire interferometry in a semi-micromechanic scale.

Various anomalous effects were observed in the displacement fields. The zig-zag fringe patterns indicated that the fiber orientation in each layer was not truly circumferential. This deviation from the unidirectionality caused free-edge effects,

such as interlaminar shear strains even at the axis of symmetry and the altered normal strains in the thickness direction. In the resin-rich zones between layers, the tensile interlaminar strain was excessively large due to the large compliance. The measured values of the interlaminar tensile strains were larger than those predicted analytically. When the free-edge effects are neglected, the only possible origin for this discrepancy is the assumption of $E_3 = E_2$. By comparison, the effective modulus E_3^{eff} is determined to be approximatey 20 % lower than the assumed value. This lower E_3 values can be explained by the interlaminar resin-rich zones arrayed in series with the plies.

The final failure of the specimen has never occurred at the maximum-stress position predicted analytically. In the semi-elliptic specimens the fracture occurred at random positions, while the semi-elliptic specimens showed a uniform manner as shown in Fig. 19.

REFERENCES

1. Guild, J., 1956, "The Interference System of Crossed Diffraction Gratings," Clarendon Press, Oxford.
2. Post, D., 1986, "Moire Interferometry," SEM Handbook on Experimental Mechanics, A.S. Kobayashi, Editor, Prentice-Hall.
3. Lekhnitskii, S.G., 1968, "Anisotropic Plates," Gordon and Breach Science Publishers, New York.

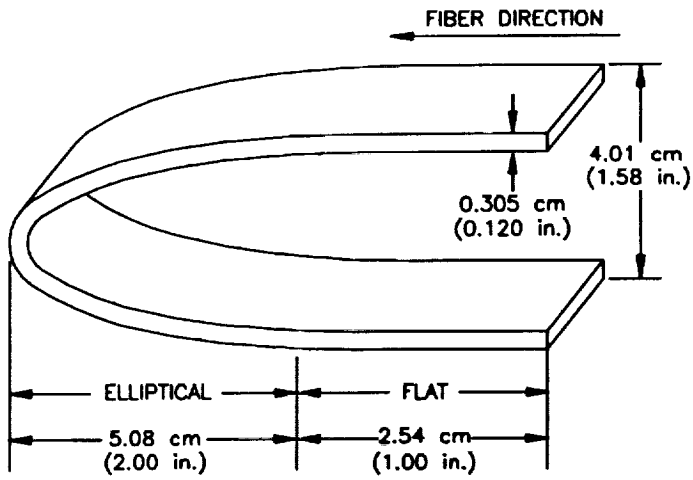

(T300/934, Graphite/Epoxy)

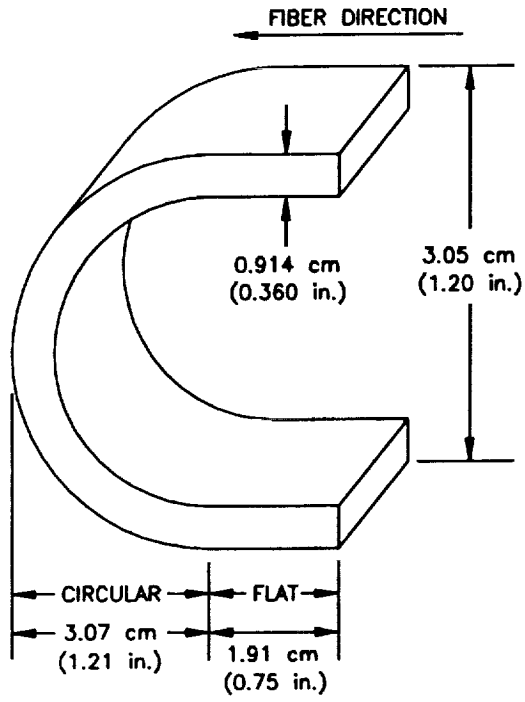

(G40–600/5245C, Graphite/Mod Epoxy)

Fig. 1. Specimens.

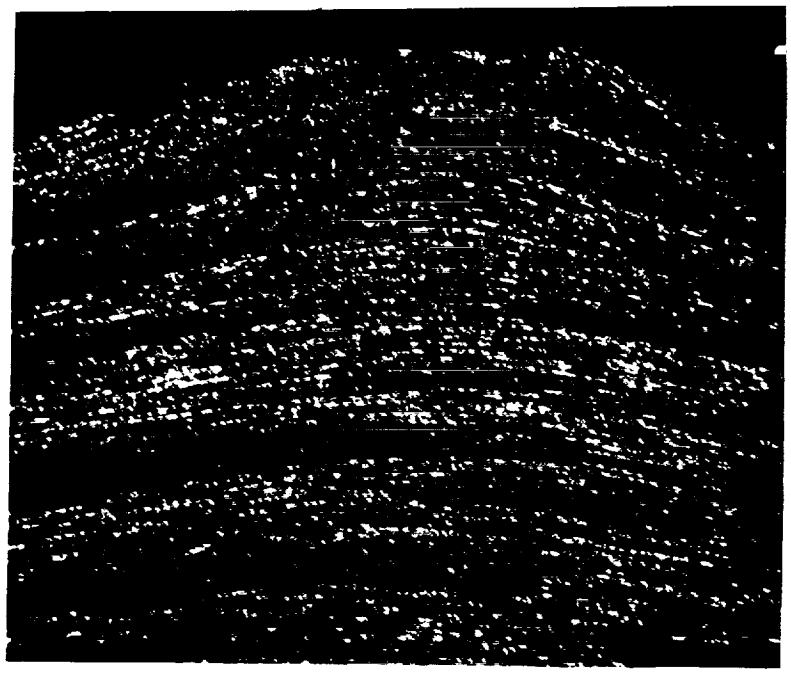

Fig. 2. Molding defect in semi-elliptic specimens near the outer edge.

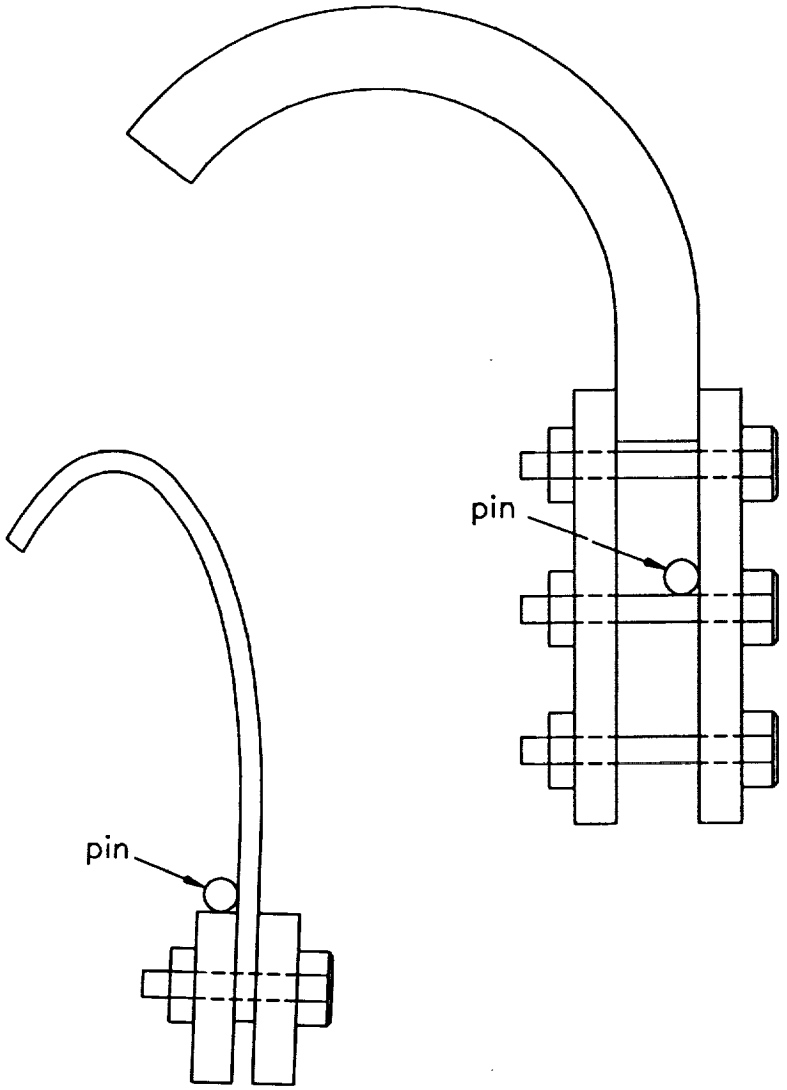

Fig. 3. Aluminum tabs attached to the specimens.

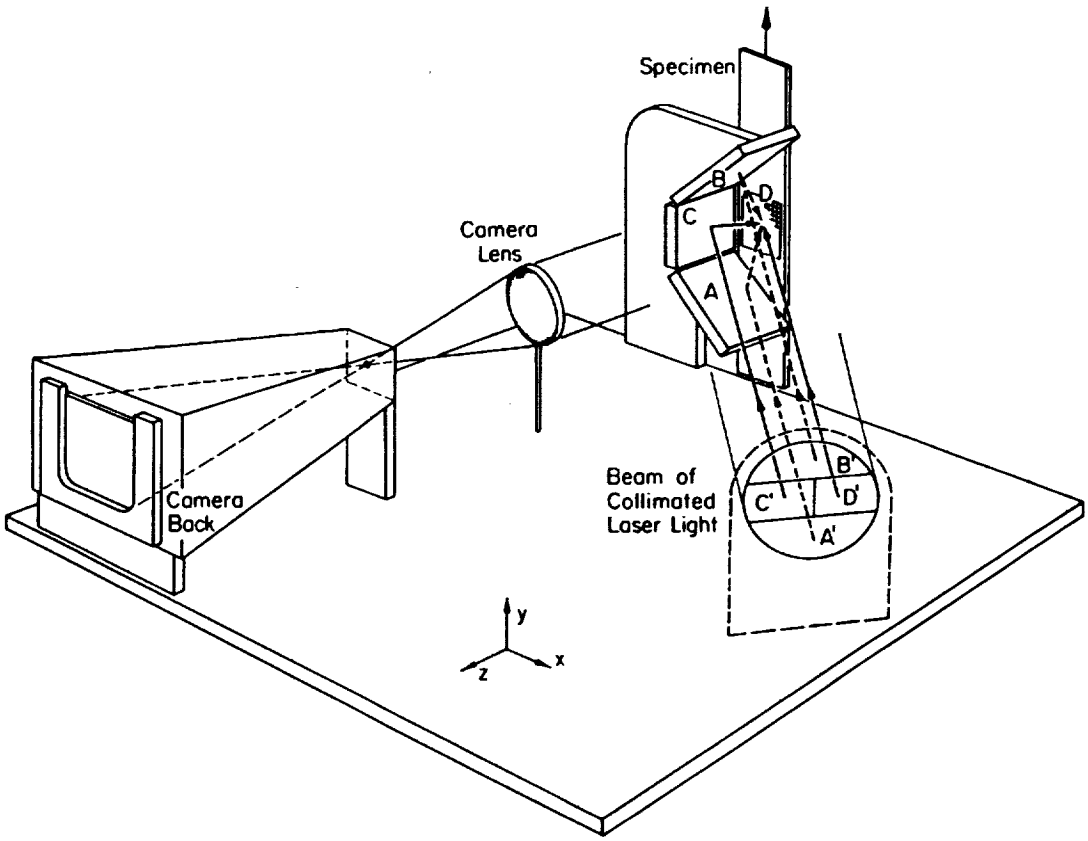

Fig. 4. High-sensitivity moire interferometer.

U

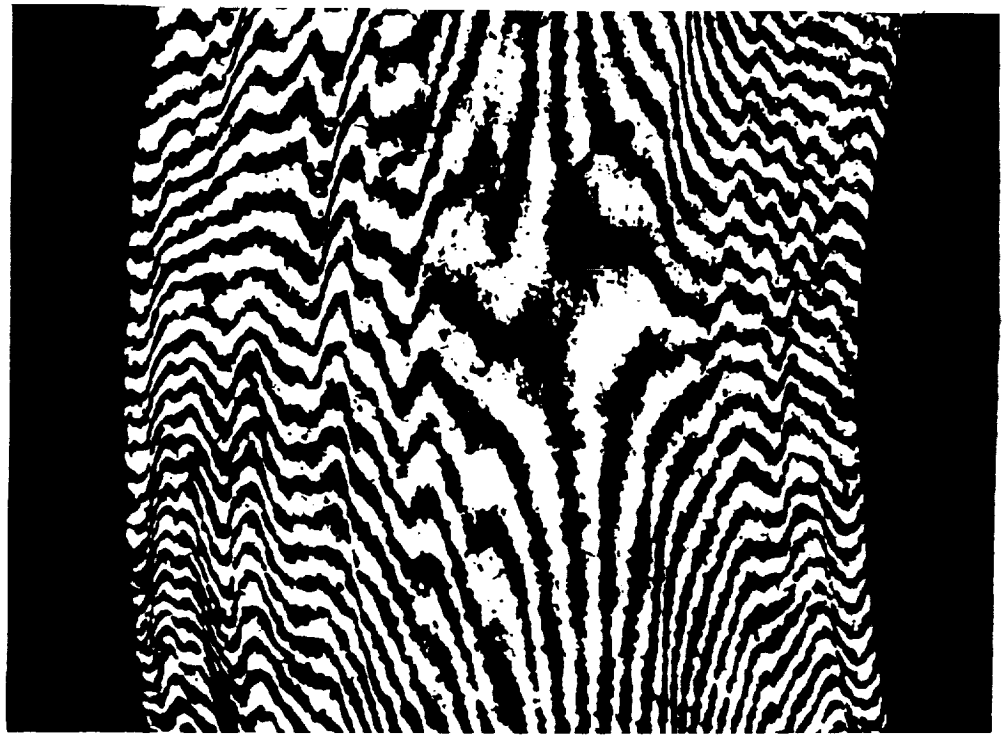

V

Fig. 5. The fringe patterns in a semi-elliptic specimen at 103 lb.

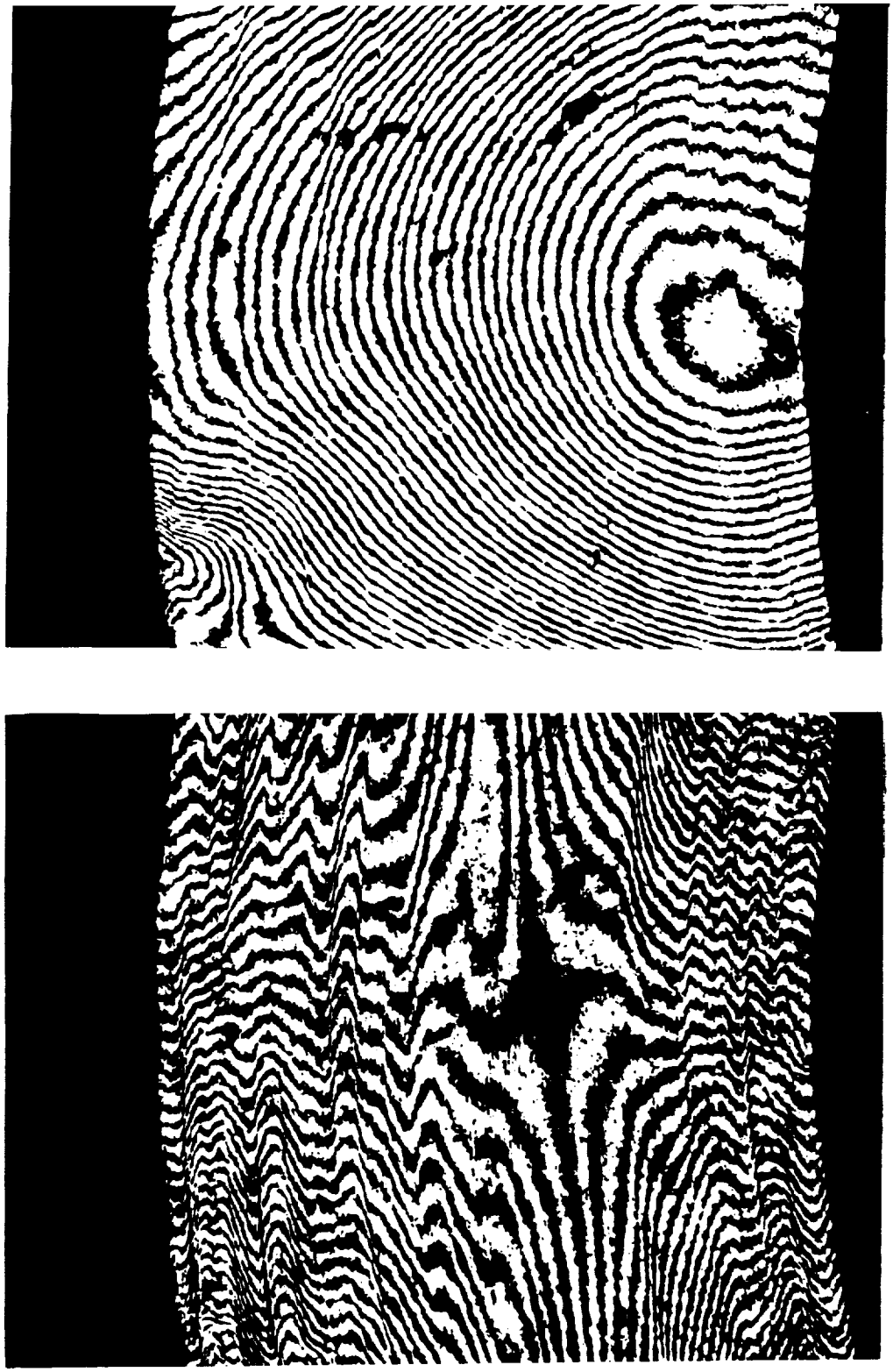

Fig. 6. The fringe patterns in a semi-elliptic specimen at 150 lb.

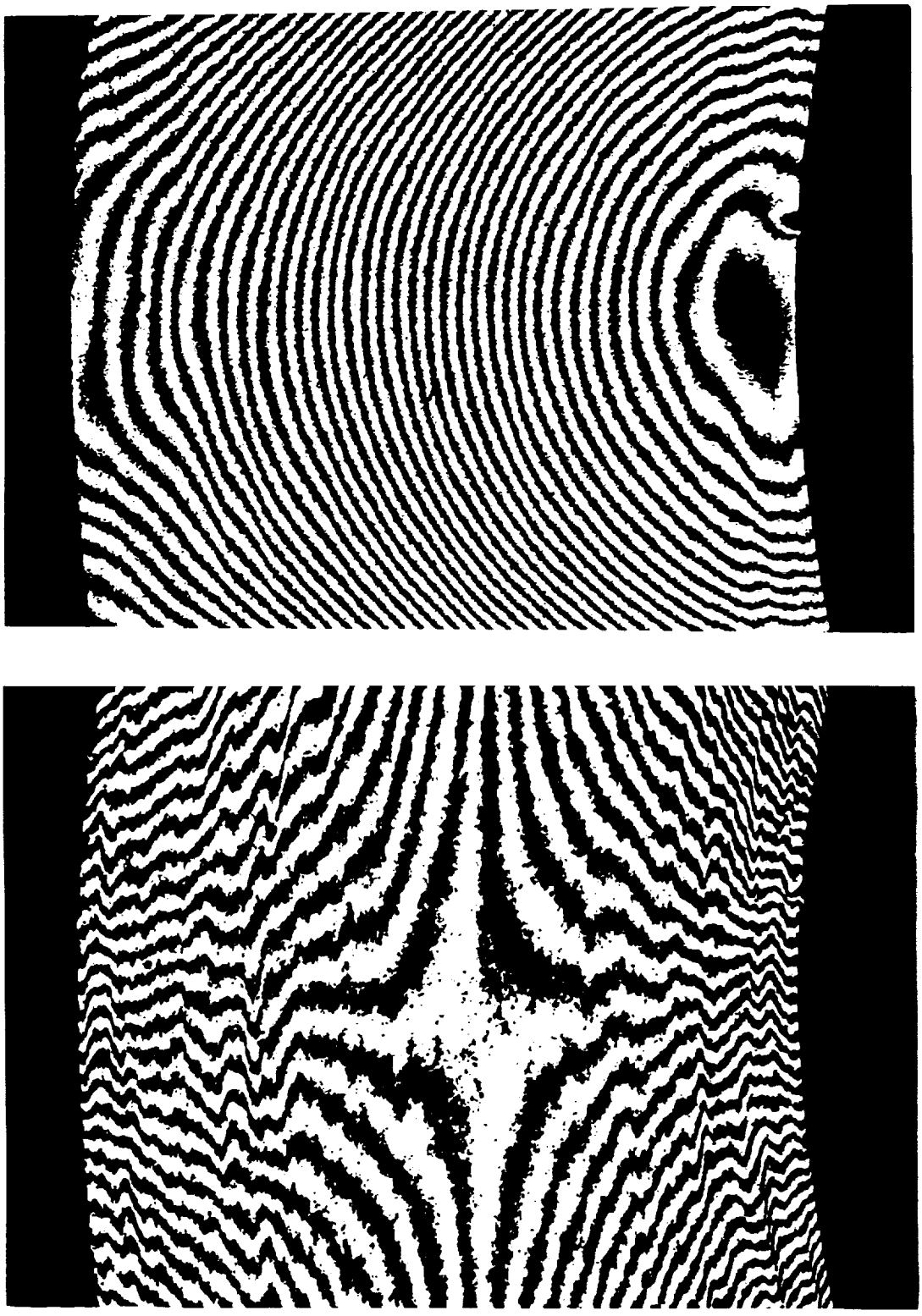

Fig. 7. The fringe patterns in a semi-circular specimen at 91 lb.

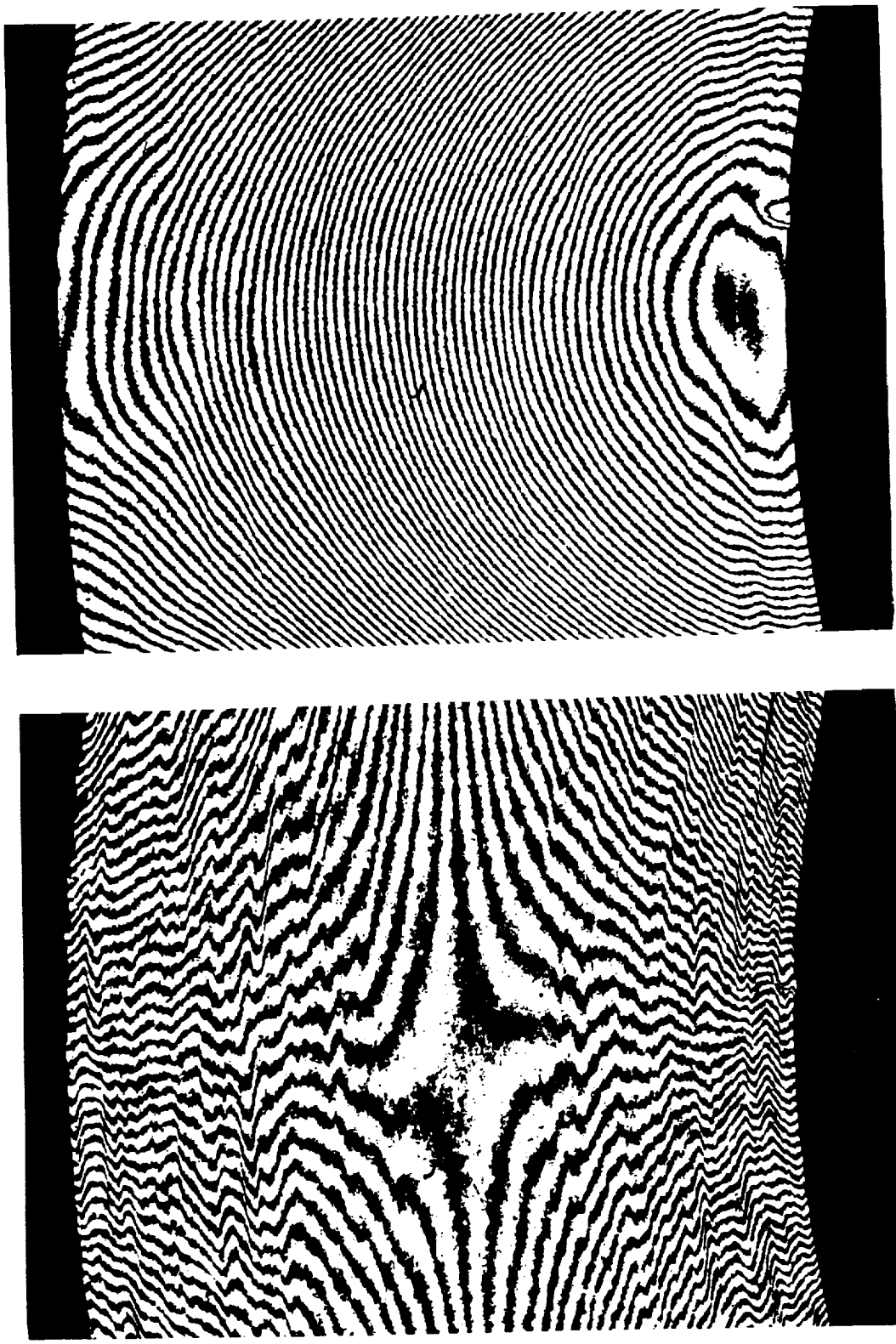

Fig. 8. The fringe patterns in a semi-circular specimen at 155 lb.

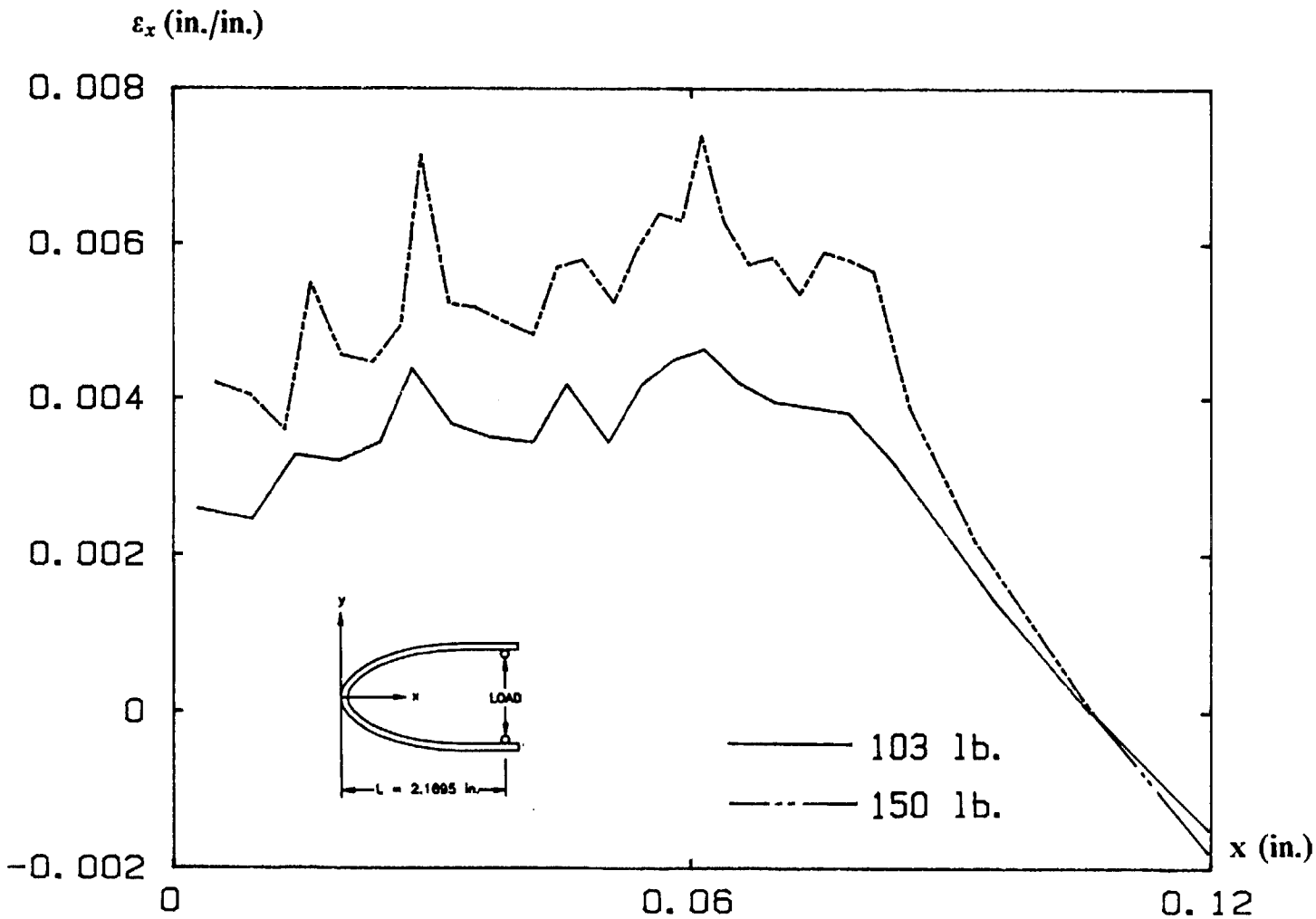

Fig. 9. The interlaminar tensile strains, ε_x, in a semi-elliptic specimen (data point connection).

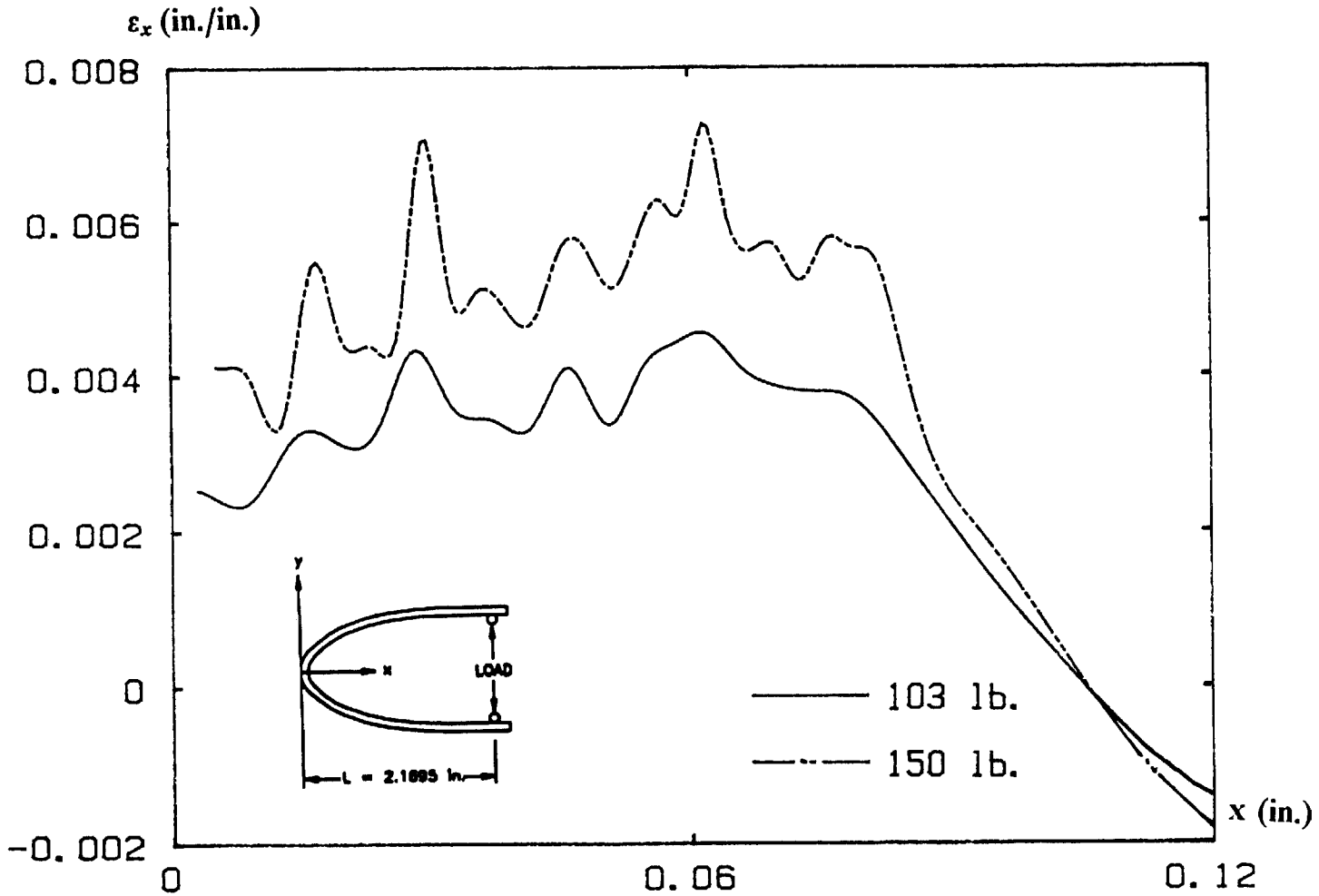

Fig. 10. The interlaminar tensile strains, ε_x, in a semi-elliptic specimen (cubic-spline method).

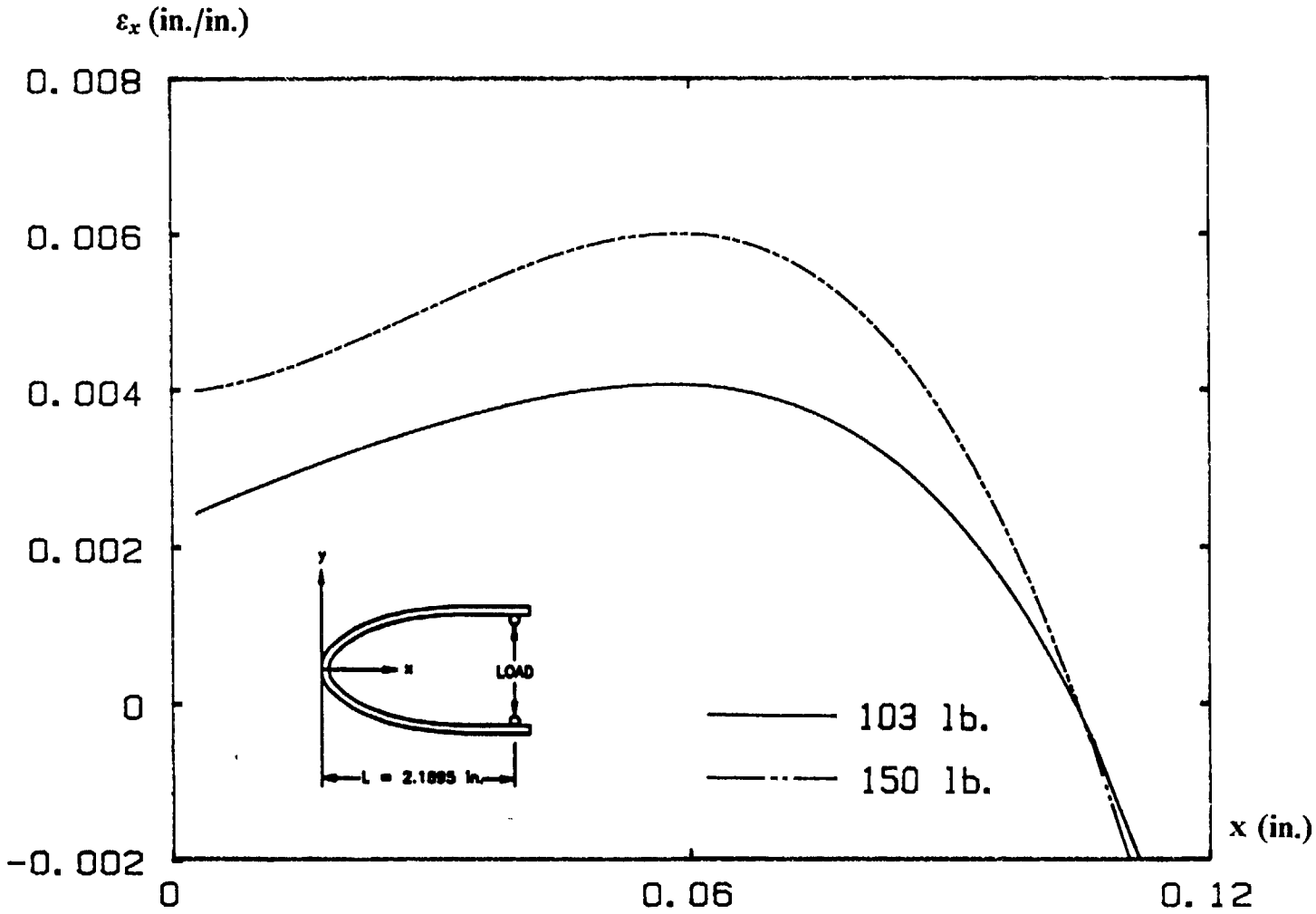

Fig. 11. The fourth-order polynomial fitting of ε_x.

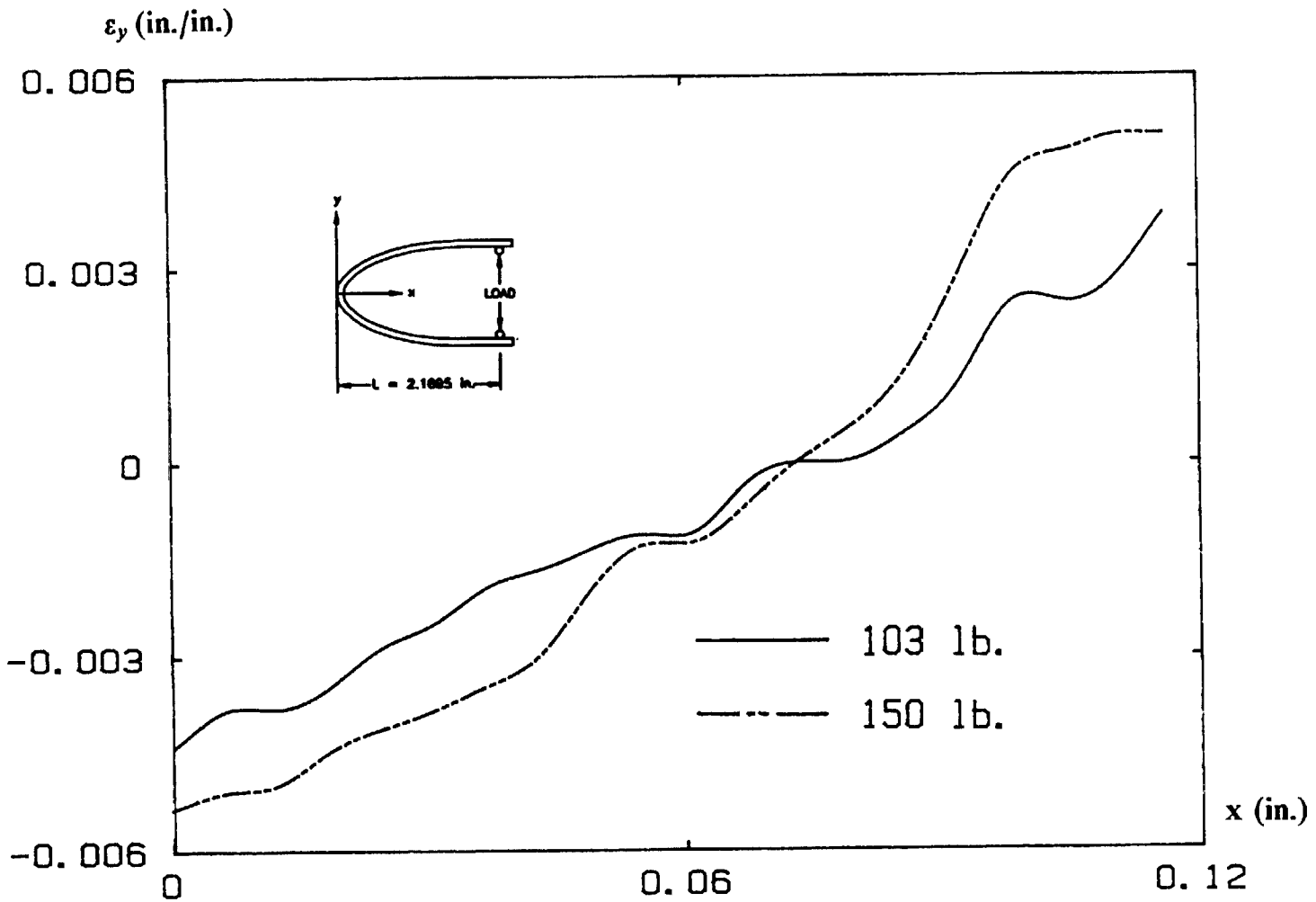

Fig. 12. The circumferential strains, ε_y, in a semi-elliptic specimen.

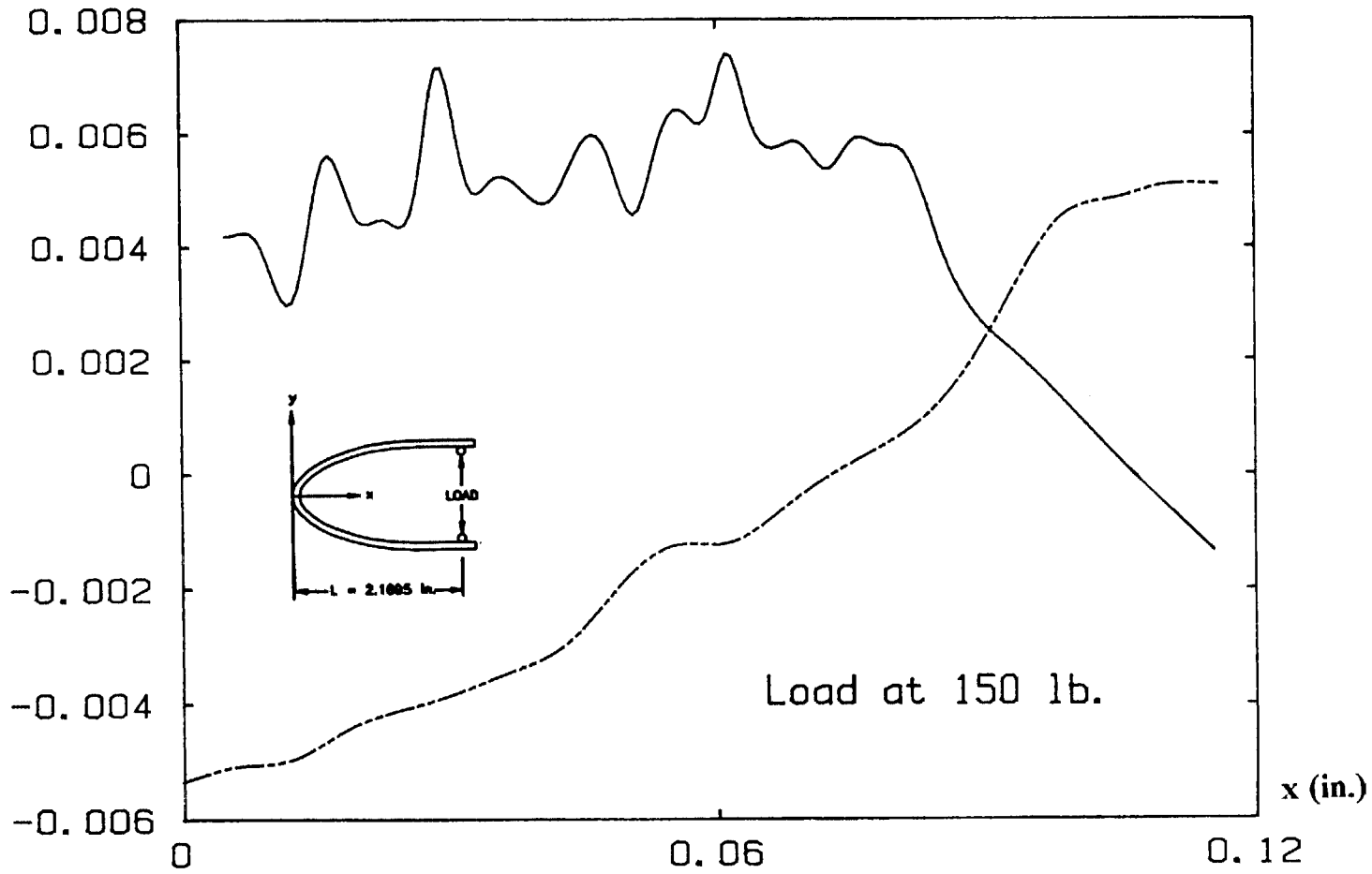

Fig. 13. The strains, ε_x and ε_y, at the same load of 150 lb.

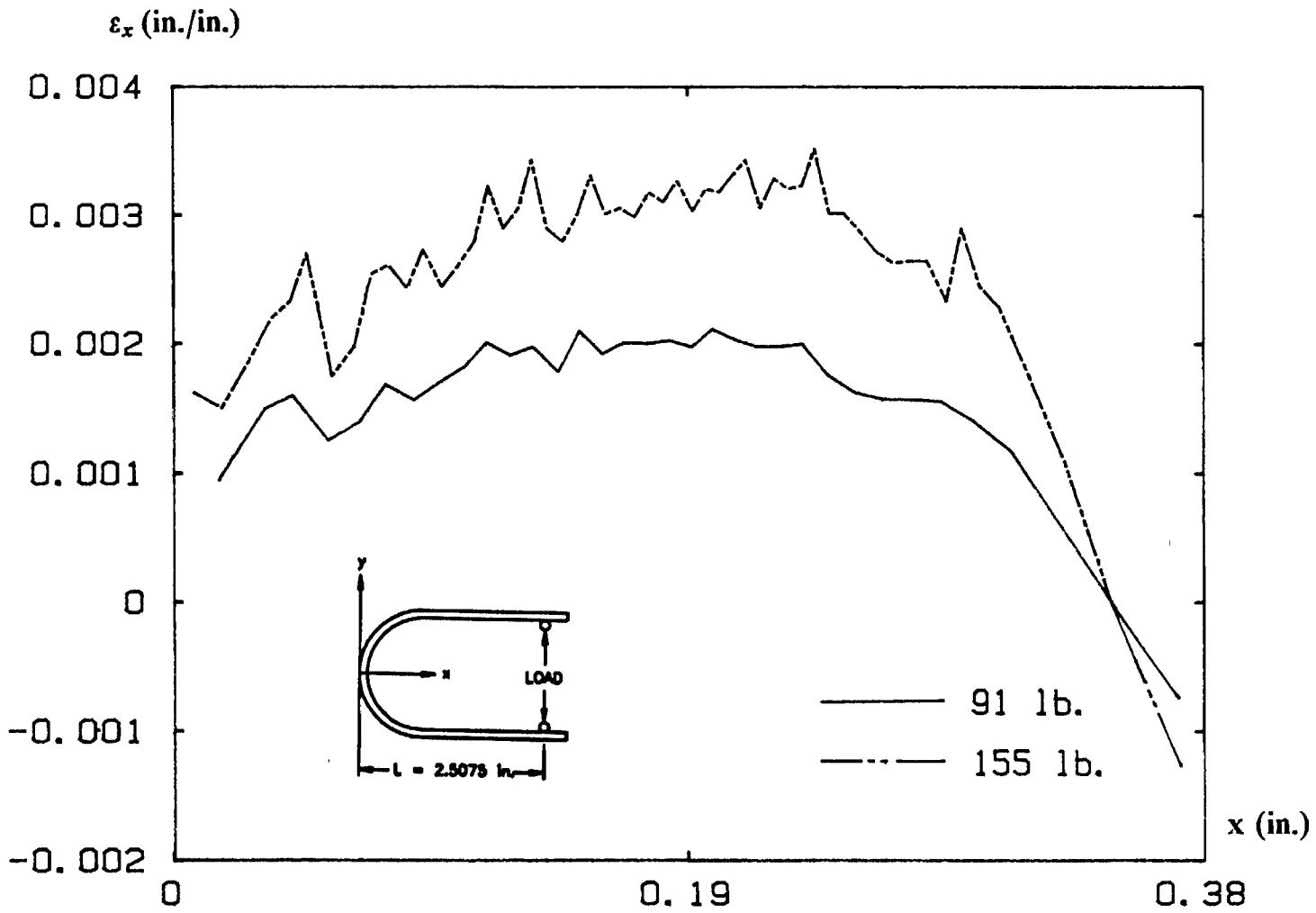

Fig. 14 The interlaminar tensile strains, ε_x, in a semi-circular specimen (data point connection).

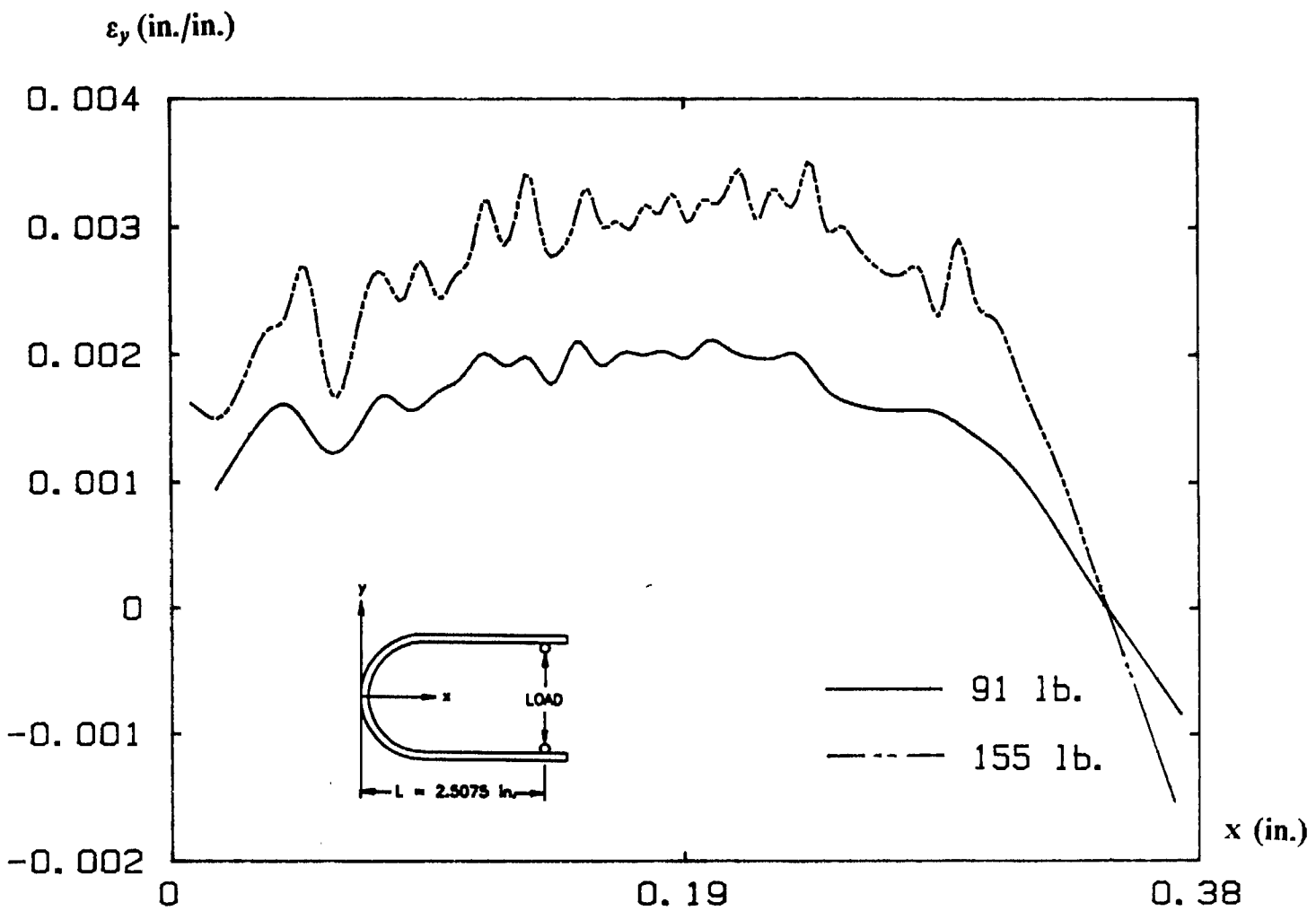

Fig. 15. The interlaminar tensile strains, ε_x, in a semi-circular specimen (cubic-spline method).

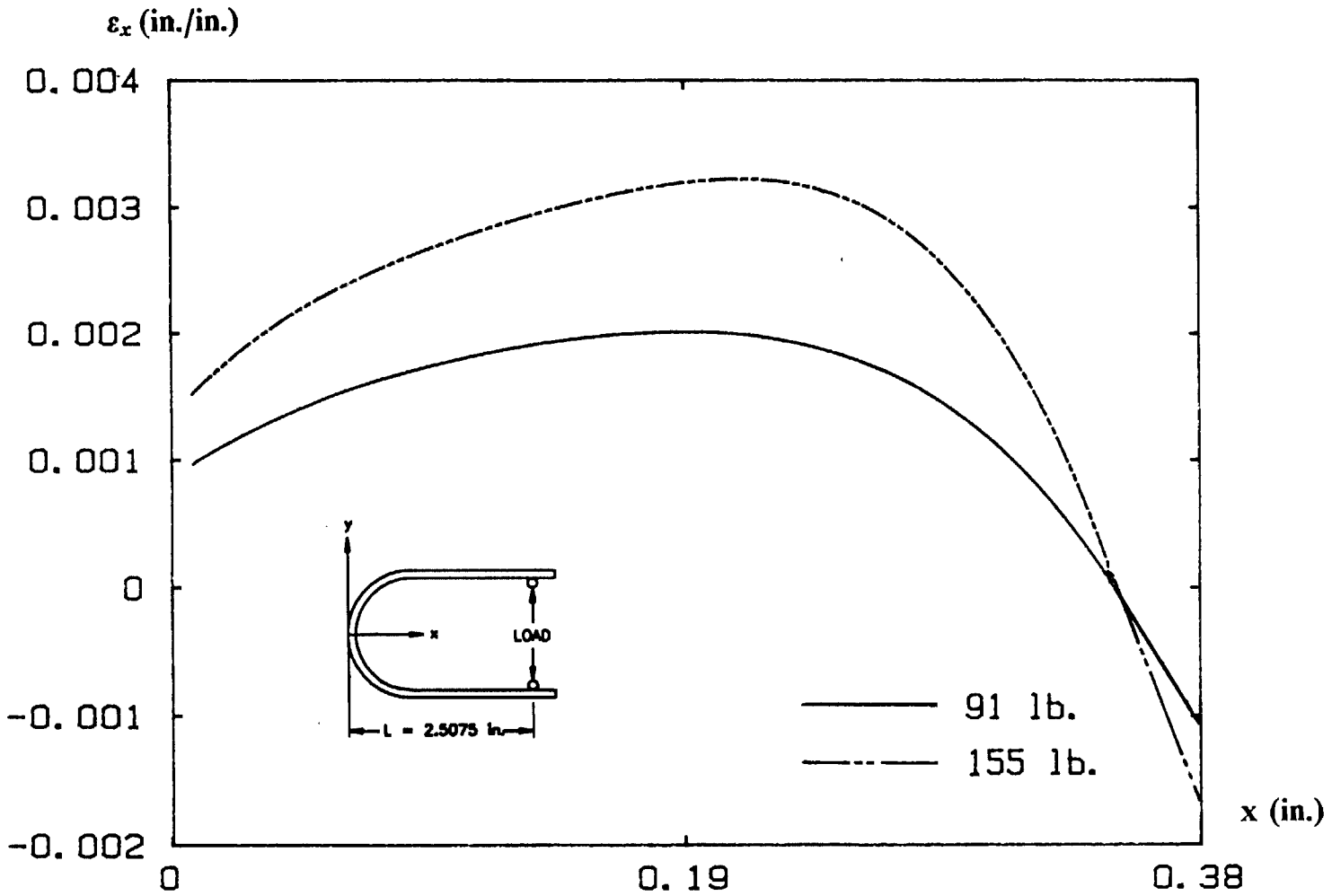

Fig. 16. The fourth-order polynomial fitting of ε_x.

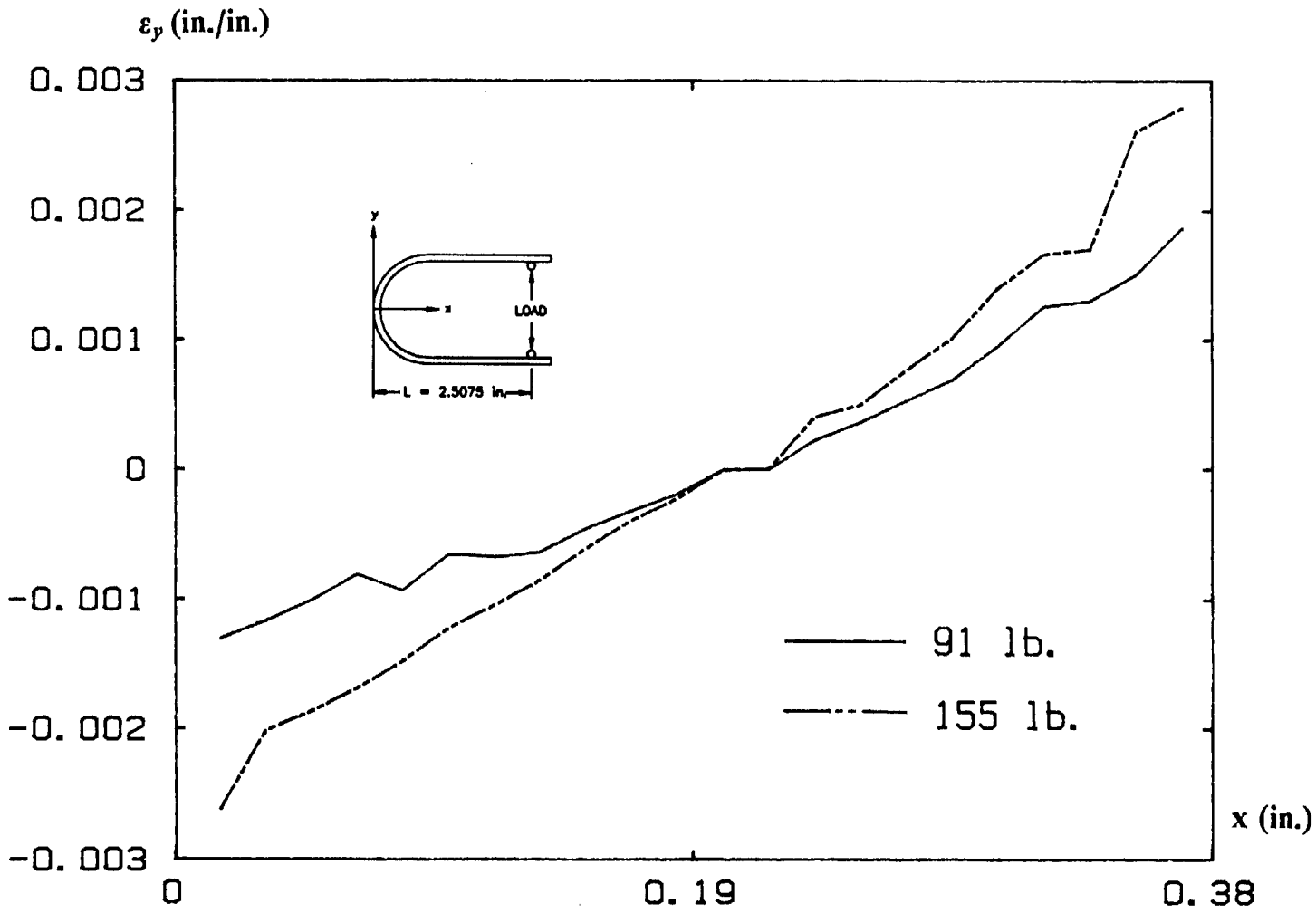

Fig. 17. The circumferential strains, ε_y, in a semi-circular specimen.

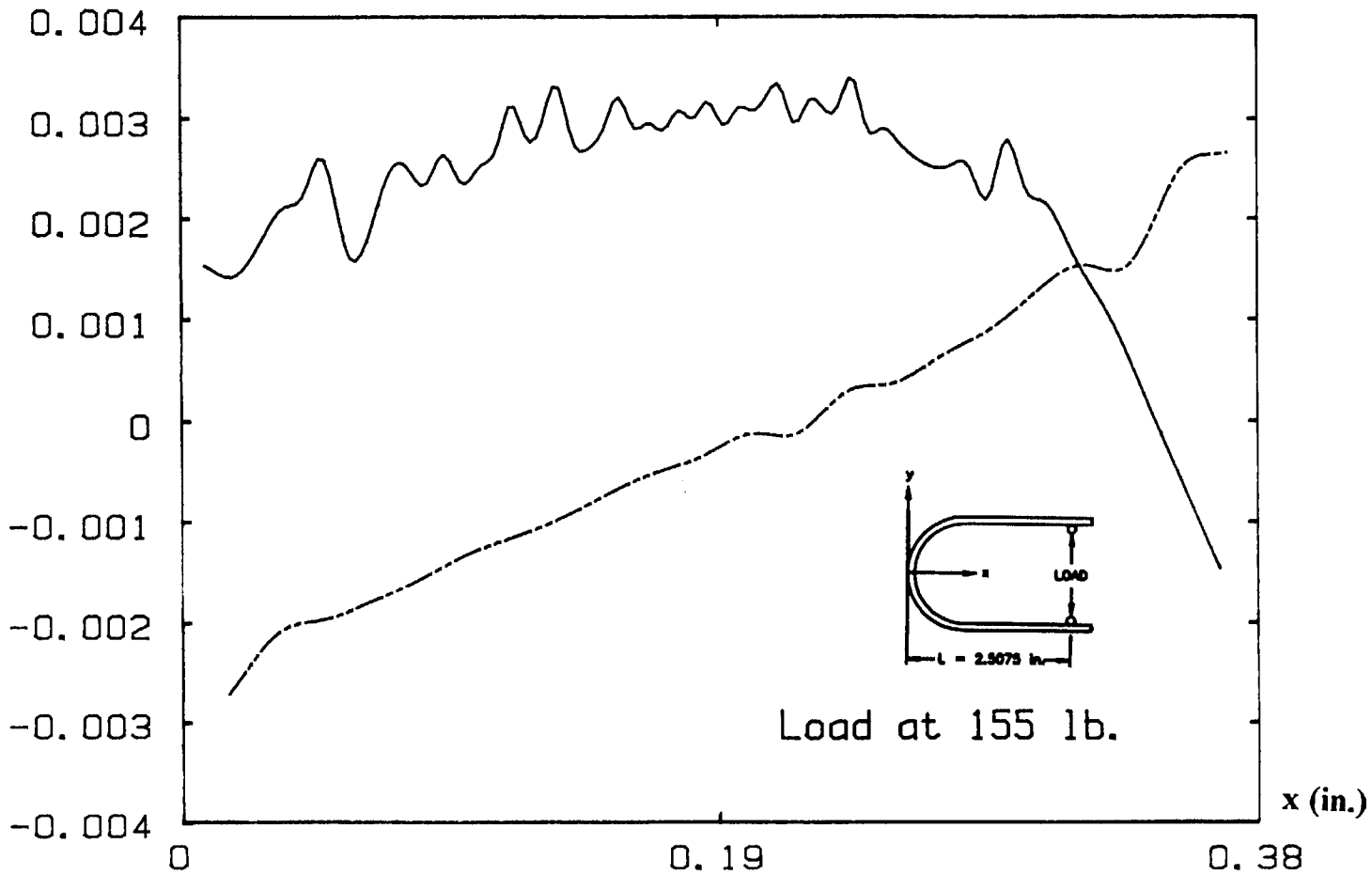

Fig. 18. The strains, ε_x and ε_y, at the same load of 155 lb.

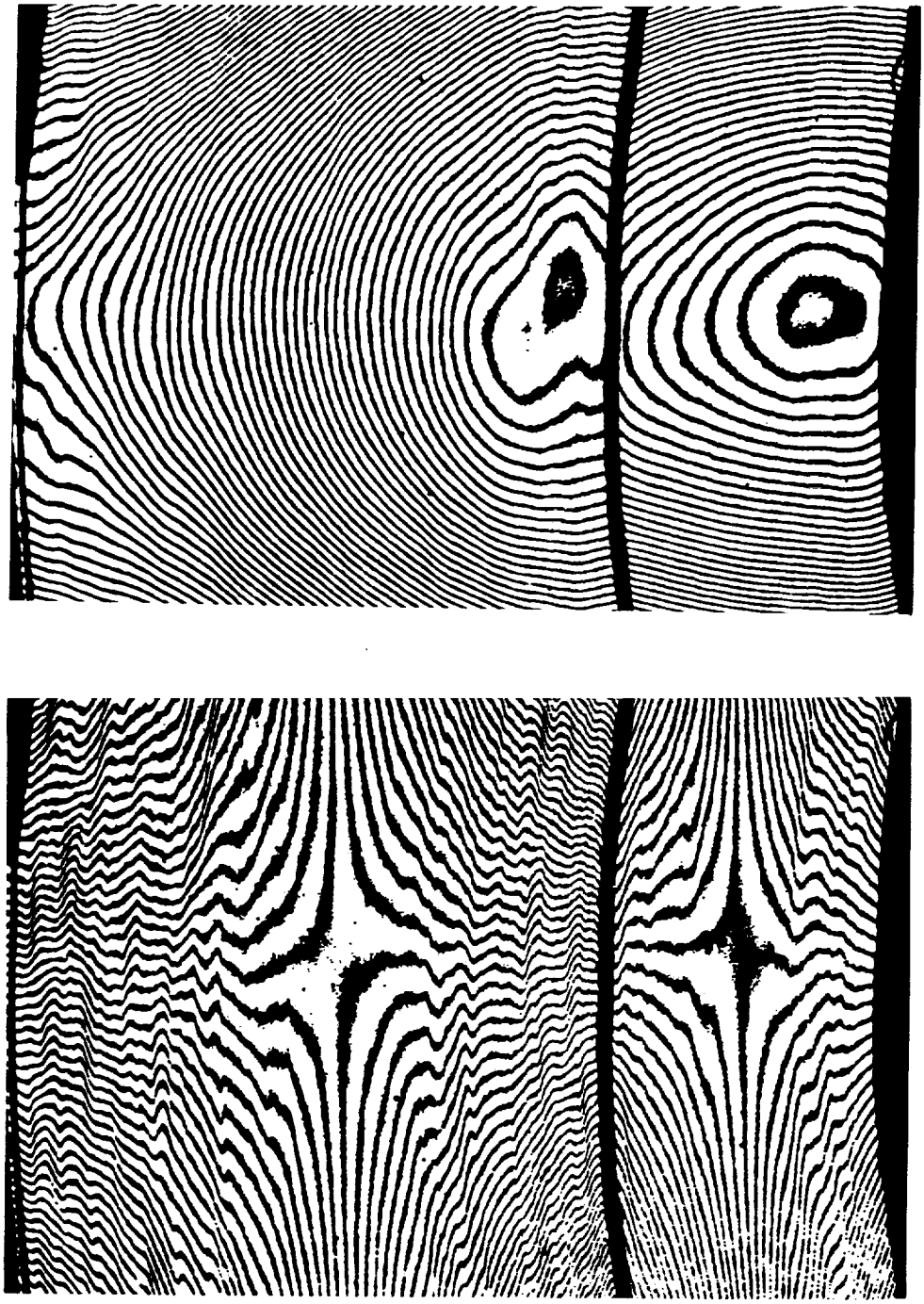

Fig. 19. Fracture mode of semi-circular specimens.